

1 **Analysing the impact of compaction of soil aggregates using**
2 **X-ray microtomography and water flow simulations**

3
4 *Menon M¹, Jia, X², Lair GJ^{3,4}, Faraj, PH¹, Blaud A¹

5
6 1. Department of Civil and Structural Engineering, KROTO Research Institute, University
7 of Sheffield, Broad lane, Sheffield S10 5SX

8 2. Department of Particle Science and Engineering, University of Leeds, LS2 9JT

9 3. University of Natural Resources and Life Sciences (BOKU), Institute of Soil Research,
10 Vienna, Peter-Jordan-Str. 82, 1190 Vienna, Austria

11 4. University of Innsbruck, Institute of Ecology, Sternwartestr. 15, 6020 Innsbruck,
12 Austria.

13
14 *corresponding author

15 Department of Civil and Structural Engineering, KROTO Research Institute,
16 University of Sheffield, Broad lane,
17 Sheffield S10 5SX,
18 United Kingdom.

19 E-mail: m.menon@sheffield.ac.uk

20 Tel: +44 (0) 114 222 5752

21
22 **Keywords:** *soil compaction, soil aggregates, X-ray microtomography, Lattice Boltzmann,*
23 *modelling, water flow*

25 **Abstract**

26 Soil aggregates are structural units of soil, which create complex pore systems
27 controlling gas and water storage and fluxes in soil. Aggregates can be destroyed during
28 swelling and shrinking or by external forces like mechanical compaction and yet, the
29 knowledge of how physical impact alters aggregate structure remains limited. The aim of
30 the study was to quantify the impact of compaction on macroaggregates, mainly on the
31 pore size distribution and water flow. In this study, aggregates (2–5 mm) were collected
32 by dry sieving in grassland of the Fuchsenbigl–Marchfeld Critical Zone Observatory
33 (Austria). The structural alterations of these soil aggregates under controlled compaction
34 were investigated with a non-invasive 3D X-ray microtomography (XMT). The detailed
35 changes in pore size distribution between aggregates (interpores, diameter > 90 μm) and
36 within the aggregates (intrapores, diameter \leq 90 μm) in pre- and post-compacted soils
37 were revealed at two soil moisture (9.3% and 18.3% w/w) and two bulk density
38 increments (0.28 and 0.71 g cm^{-3} from the initial values). The soil permeability was
39 simulated using lattice Boltzmann method (LBM) based on 3D images. Soil compaction
40 significantly reduced total pores volume and the proportion of interpores volume and
41 surface area, while total pore surface area and the proportion of intrapores volume and
42 surface area increased. The increases in soil moisture tended to reduce the effects of
43 compaction on interpores and intrapores, while the high compaction increment
44 drastically changed the pore size distribution. The aggregate compaction decreased
45 water penetration potential due to the increase of small intra-aggregate pores and
46 cavities as demonstrated by LBM. Notably, the LBM results showed a significant linear
47 correlation between the water flow rate and bulk density of soil aggregates and predicted
48 that the water flow could be reduced by up to 97–99% at bulk density of \geq 1.6 g cm^{-3} with
49 soil water content of 18.3% w/w. Thus, a combination of imaging and modelling provided

50 new insights on the compaction effects on aggregates, underpinning the importance of
51 protecting soil structure from mechanical compaction to minimise environmental
52 impacts of soil compaction and maintain water infiltration and percolation in arable soils.

53

54 **1. Introduction**

55 Aggregates are the structural units of soils with different size and shape, and are
56 formed by the agglomeration of mineral particles (i.e. clay, silt and sand) and a variety of
57 binding agents such as roots, fungal hyphae and microbial polysaccharides, calcium
58 bridges and different (hydr) oxides (Six et al., 2004; Tisdall and Oades, 1982). The
59 structure and stability of aggregates is crucial for water infiltration and movement, gas
60 exchange, soil erosion, biological activity and rooting influencing the growth of crops
61 (Hillel, 1998; Amézqueta, 1999; Bronick and Lal, 2005). Soil compaction is the
62 densification of soil by application of mechanical energy (Holtz et al., 2010), which can
63 occur naturally or driven by anthropogenic activities. The result is an increase of bulk
64 density and a reduction of pore space, affecting the percolation of soil water as well as
65 gas exchange or production. Soil compaction has been strongly linked to the loss of
66 nitrogen by the accelerated production of greenhouse gases (e.g. N₂O) through
67 denitrification in anaerobic conditions (Keller et al., 2013). Due to above ecological
68 impacts, soil compaction has been widely recognized as a soil threat by many regional,
69 national and international organisations (Hartemink, 2008; Banwart, 2011). It has been
70 described as an ‘unnecessary form of land degradation’ by Food and Agricultural
71 Organization (FAO, n.d). In Europe, compaction is widespread and it accounts for about
72 17% of the total area of degraded soil (EEA, 2012). The EU Soil Thematic Strategy
73 identified compaction as one of the major soil threats in Europe (COM, 2006).

74 Most of the studies investigating soil compaction were conducted using bulk soils
75 under lab or field conditions. However, the compaction of soil aggregates was rarely
76 investigated despite the fact that the size distribution of aggregates has been often used
77 as an indicator of soil fertility. For example, an empirical rule suggests that a soil structure
78 consisting of more than 60% of macro-aggregates (0.25–10 mm) can be classified as
79 “agronomically valuable” (Shein, 2005). The size and stability of soil aggregates regulate
80 gas and liquid diffusion in soil (Sexstone et al., 1985; Horn and Smucker, 2005), enhance
81 the accumulation of soil organic matter by physical protection (Bossuyt et al., 2002),
82 provide specific microbial habitats and directly influence microbial composition and
83 activity (Blaud et al., 2012). However, soil aggregates turnover (i.e. cycles of formation
84 and natural disruption of aggregates) (Stamati et al., 2013) is easily disturbed in presence
85 of external factors such as tillage or compaction. In particular, macroaggregates
86 (diameter > 0.25 mm) are disrupted the most. However, there is a limited mechanistic
87 understanding how breakdown of macroaggregates occur and how this can affect the
88 movement of air and water in soils.

89 Dexter (1988) proposed three main changes in soil aggregate structure during
90 compaction depending on soil moisture content. Firstly, when soil aggregates are dry and
91 hard, the soil particles will be rearranged under compaction. Secondly, when aggregates
92 are weak or brittle, fracture will occur and broken aggregates fragments may fill up the
93 spaces between existing soil aggregates and particles. Thirdly, aggregates are plastic
94 (depends on moisture content) and when compacted, the compression creates plastic
95 flow with flat areas of contact between the aggregates. However, the dynamics of pore
96 space in these scenarios are to be studied in order to produce meaningful predictions on
97 water or air flow; i.e. further insights are needed on how compaction affect the internal

98 (intra-aggregate pores or intrapores) along with changes in porosity between them
99 (inter-aggregate pores or interpores) as well as overall pore size distribution.

100 Compaction is a multidisciplinary problem and several methods can be used to
101 study structural alterations in soils. Thus, a selection of method for studying compaction
102 will depend on the research context and resources available (see review from Keller et
103 al., 2013). Total porosity can be calculated by measuring bulk density and the soil density
104 in laboratory. Odometer is also used widely to study compaction. However, these
105 methods do not provide information about pore size distribution in the sample and for
106 this, the soil water retention curve has to be measured using the pressure plate
107 apparatus. Imaging tools can yield high resolution 2D or 3D images of pore space. For 2D
108 imaging, thin sections are made from resin impregnated soil samples and images are
109 processed for different pore characteristics (Murphy, 1986). This method suffers from
110 the problem of destructive sampling, and cross sections do not provide information on
111 the real 3D geometry of the pores in samples. In contrast, using the advanced 3D imaging
112 tools such as XMT (X-ray microtomography, also known as micro-CT) and image analysis
113 software, it is now possible to study the pore size characteristics with very high spatial
114 resolution (up to a few microns, depending on the sample size) non-destructively
115 (Mooney et al., 2012). In addition, the data from XMT can be directly used for modelling
116 to quantify processes such as diffusion of fluids. However, imaging methods suffers from
117 the fact that the resolution depends on the sample diameter. Despite its several
118 advantages, it has not been used widely to study soil compaction. Few studies have
119 already demonstrated the water flow through aggregates using 2D images (Aravena et
120 al., 2014; Berli et al., 2008; Carminati et al., 2007). Notably, Aravena et al. (2014) showed
121 that root-induced compaction led to deformation of aggregates and subsequent reduction
122 in inter-aggregate porosity (or increased inter-aggregate contact areas), which increased

123 the unsaturated flow of water towards the root by 27%. However, above studies used 2D
124 image slices and the dynamic of intra-aggregate pore space was not evaluated. An
125 alternative modelling method is available, that uses 3D image data is Lattice Boltzmann
126 Method (LBM), which is simpler and faster and do not require finite element meshing of
127 images as demonstrated earlier by Menon et al. (2011).

128 The aim of this laboratory study was to investigate the impact of compaction on a
129 pack of soil aggregates on its pore structure and water flow with the following specific
130 objectives: (1) visualize and quantify inter- and intra-aggregate pores in compacted soils,
131 (2) compare the effect of soil moisture content and different compaction strengths on the
132 pore size characteristics (inter and intra aggregate porosities and pore volume
133 distribution) of soil aggregates, (3) predict the effect of compaction on water flow using
134 LBM. We hypothesise that the deformation of aggregates due to soil compaction increases
135 with soil moisture content and compaction level, leading to a decrease in water flow and
136 pore space which is directly related to the dynamics of inter- and intra-aggregate pores.

137

138 **2. Materials and Methods**

139 *2.1. Soil sampling and preparations*

140 Dry sieved soil aggregates were collected from bulk soil below the main rooting
141 zone (5–10 cm soil depth) at an agriculturally used grassland site located in Fuchsenbigl–
142 Marchfeld Critical Zone Observatory in September 2011. The field site is located east of
143 Vienna, Austria, in the National Park “Donau-Auen” and developed on approx. 350 year
144 old alluvial Danube River sediments (48°11’N, 16°44’E; Lair et al., 2009). The soil
145 aggregates distribution of bulk soil (5–10 cm soil depth) obtained by wet sieving (Haynes
146 and Swift, 1990) revealed the following aggregate size distribution: <0.25 mm (6.1%),
147 0.25–0.5 mm (6.9%), 0.5–1 mm (5.2%), 1.0–2.0 mm (14.5%), 2.0–5.0 mm (37.8%) and 5–

148 10 mm (21.5%). More than 90% of the aggregates were water stable. Therefore, the
149 predominant aggregate size class of 2–5 mm was selected for this study. Particle size
150 distribution in this aggregate size class was 78 g kg⁻¹ sand, 644 g kg⁻¹ silt and 278 g kg⁻¹
151 clay. The organic C concentration was 49.0 g kg⁻¹ and total N 33.8 g kg⁻¹ in the studied
152 aggregates.

153 To study the effect of soil compaction, samples were prepared with two different
154 moisture levels: (1) aggregates with gravimetric water content of 9.3% (W1),
155 representing the field moisture content at the time of sampling, and (2) an elevated
156 moisture content of 18.3% (W2), at which aggregates were only slightly plastic and thus
157 easier to handle in imaging experiments. For the latter, the aggregates were saturated
158 with water first and air-dried until the desired soil moisture was attained. Soil aggregates
159 were weighed and filled into a specially designed plastic cylinder (14.9 mm inner \varnothing and
160 60 mm height) with a piston. The size of the plastic cylinder was particularly selected in
161 order to fit (sample size limits for the imaging device: 60 mm length and 50 mm diameter)
162 the imaging device as well as to achieve a resolution of 10 mm. The bottom of the
163 container was sealed with a flat metal sheet. Three replicated samples were used for the
164 two moisture and compaction levels, respectively, using the same weight (4.14 g for W1
165 and 4.84 for W2) of aggregates. Soil aggregates were filled and gently tapped to settle the
166 aggregates in the cylinder and the initial bulk density was calculated using the mass–
167 volume relationship. All samples were imaged before compaction to get initial pore
168 structure (details on imaging is provided in the following section) and then compacted
169 by pushing the soil by hand with the help of small piston (custom made to fit the cylinder)
170 with occasional pounding to achieve the required bulk density increment of 0.28 (BD1)
171 and 0.71 g cm⁻³ (BD2). Due to the multiple impacts involved, we could not precisely
172 measure the load applied on the samples. In order to measure the maximal approximate

173 load applied, a separate uniaxial load testing was carried out using a mechanical tester
174 (Instron, model: 5566). Maximal loads required to reach W1BD1 and W2BD1 were 185
175 (± 1.8) kPa and 116 (± 2.6) kPa, respectively, and for W2BD2 it was 530 (± 11) kPa.

176 The high compaction level (BD2) was only performed on samples with gravimetric
177 water content 18.3% (W2), because they were more compressible than the ones at lower
178 soil water content (W1). Samples were imaged again after applying compaction. Table 1
179 shows the treatment combinations, bulk densities and the maximal load applied.

180

181 *2.2. Imaging and Image Processing*

182 X-ray microtomography (XMT) has become a popular tool to characterize soil
183 structure in recent years. The method has been previously used to study pore structure
184 under mechanical disturbance of fragile biological crusts (Menon et al., 2011) and a
185 similar methodology was followed in this study. Pre and post-compacted samples were
186 imaged using XMT at 10 mm resolution (Model: Skyscan 1172 with a detector array of
187 2000 x 1048 pixels) available at the University of Sheffield. Images were reconstructed
188 and processed with Simpleware (v6) with a final effective pixel resolution of 30 mm to fit
189 the capacity of the desktop system (16GB RAM with i7 quad core processor).

190 The pores were divided into two main groups based on their size and location: (1)
191 inter-aggregate or interpores, which are the pores between soil aggregates, (2) intra-
192 aggregate pores or intrapores within soil aggregates (pores within the solid matrix of soil
193 aggregates which are mostly $< 90 \mu\text{m}$ in size). This size was selected based on several
194 preliminary image analyses of the data from the pre-compacted samples. It should be
195 noted that intrapores also include a small fraction of pores between contact surfaces of
196 aggregates but they are impossible to exclude in 3D volume image processing.

217 In order to separate inter- and intrapores, the following simple steps as shown in
218 Fig. 1 were followed. First step of image processing is the segmentation of images using
219 an appropriate pixel threshold to separate solids and pores. A floodfill operation (i.e. it
220 joins the regions with similar pixel values) was then carried out. A median filter (2 pixels)
221 was then applied to remove the noise in the image, resulting a 'soil mask'. To separate the
222 intrapores a morphological close filter (3 pixels, 90 μm) was applied to produce 'soil solid
223 mask' (i.e. closure of all intrapores) and intrapores can then be quantified by Boolean
224 image subtraction operation (i.e. intrapores = soil solid mask - soil mask). A separate
225 cylinder mask was then created to represent the sample volume in order to quantify the
226 interpores, for which the Boolean subtraction operation was used again (i.e. interpores =
227 cylinder mask - soil solid mask).

228 Although the entire length of most cylinders were scanned, it was computationally
229 challenging to process entire length (unable to upload full dataset on Simpleware) and
230 therefore top 1 cm and bottom 0.8 cm (the length of W2BD2 treatment after compaction
231 was 1.8 cm and hence was used for all samples for uniformity) of each sample were used
232 for further processing. However, after the image analysis of both parts of the columns
233 separately, it was found that the inter- and intrapores volume and surface was not
234 significantly different between the top and bottom part of the samples. Thus, the average
235 of the top and bottom were used for the figures presented in this study and for statistical
236 analysis.

237 The outputs of the analysis gave the total volume (mm^3) and total surface area
238 (mm^2) for inter- and intrapores which were also expressed as the proportion of the total
239 pore volumes or surface area per sample in the paper. This was done because of the
240 change in total volume of samples after compaction (Table 1). Further- more, from these
241 images, it was possible to quantify individual pore volumes and to present the pore

222 volume distributions before and after soil compaction. However, it was only possible to
223 count individual interpores and its volume; the software could not handle these tasks for
224 intrapores. This is presumably due to the large number of intrapores created in
225 compacted soils compared to interpores.

226

227 *2.3. Modelling Flow using Lattice Boltzmann Method (LBM)*

228 More details on this method can be found in earlier publication (Menon et al.,
229 2011), only a brief account of relevant aspects of the LBM model (code: D3Q19) is given
230 here. It is highly effective in trend analysis and compared with conventional
231 computational fluid dynamics (CFD) models, LBM is simpler and faster when used to
232 calculate flow through a complex network of pores obtained from 3D images. Its
233 simplicity is partly due to its formulation which is based on a regular (Cartesian) lattice
234 grid – the same type employed in 3D imaging. Its speed is largely also due to the same
235 reason, since no meshing or re-meshing step is required (which could take much longer
236 than the actual flow calculations). Typically, through rescaling in the model formula-
237 tion, LBM input and output are expressed in lattice units. For example, length is specified in lu
238 (length unit), time in ts (time step), velocity in $lu\ ts^{-1}$, and kinematic viscosity in $lu^2\ ts^{-1}$.
239 Nominally, both lu and ts are set to 1 to simplify calculations. LBM simulations are usually
240 performed in a setup that helps to ensure numerical stability, then the results are rescaled
241 to match the required, for instance, superficial velocity by taking advantage of the laws of
242 similarity in fluid mechanics. LBM is known to be applicable only in low Mach numbers.
243 It is assumed that flow pattern remains the same within a certain range of Reynolds
244 number (e.g. creeping flow regime). To convert between lattice units and physical units,
245 it is usually assumed that dimensionless ratios such as Reynolds number or drag force
246 coefficient are equal across the different (LBM and physical) systems. Take superficial

247 velocity as an example, if $Re (=UL/v)$ is assumed to be equal, the following equation can
248 be used to convert LBM calculated velocity in lattice units to real velocity in physical units:

$$249 \quad U_{phys} = \frac{v_{phys}}{L_{phys}} Re_{lattice} = \frac{v_{phys}}{L_{phys}} \frac{U_{lattice} L_{lattice}}{v_{lattice}} \quad (1)$$

250 where L is a characteristic length, τ a relaxation parameter in LBM and is related to
251 kinematic viscosity by $\nu = (2\tau-1)/6$. In practice, τ is typically set to 1 and was the case in
252 those current simulations. The driving force for flow in our LBM implementation is a user-
253 definable, constant body force, f_b . Its value is typically set to a value below 0.015 for the
254 sake of numerical stability. In our simulations it was set to 0.001. A constant body force
255 is equivalent to a constant pressure gradient throughout the domain. Fluid density is
256 customarily set to a nominal value of 1. During a LBM simulation, calculated superficial
257 velocity is monitored and the simulation was stopped once this value became stable over
258 a few hundred steps.

259 The final superficial velocity in physical units is equivalent to Darcy hydraulic
260 conductivity. Permeability, as defined in Darcy law, is calculated using LBM input (ρ , ν
261 and f_b) and output (U) as

$$262 \quad K = \frac{U \rho \nu}{f_b} \quad (2)$$

263 It has the units of lu^2 .

264 The LBM simulations were carried out only for elevated moisture level (18.3%)
265 treatment because three bulk density levels were available (0.9, 1.2 and 1.6 g cm⁻³). Due
266 to small sample size and nature of this study (e.g. samples were imaged in pre and post-
267 compacted condition), it was nearly impossible to measure the hydraulic conductivity in
268 order to compare the results from modelling.

269

270 *2.4. Statistics*

271 The effect of soil compaction on soil pores (total pores, interpores and intrapores)
272 volume and surface area was investigated using paired Student's t-Test (as the porosity
273 of the same samples was measured before and after soil compaction). The effects of soil
274 moisture level and compaction level were investigated using unpaired Student's t-test.
275 All the statistical analyses were performed using R version 3.1.0 (R Development Core
276 Team, 2013).

277

278 **3. Results**

279 *3.1. Visualization of Pore Characteristics*

280 Reconstructed images from XMT were processed using 3D imaging tools to
281 visualize and quantify pore characteristics following the protocol described earlier (Fig.
282 1). Fig. 2 shows a comparison of aggregates (top 1 cm) before and after compaction in 3D
283 with respect to its changes in solid phase and pore space (inter- and intrapores) of the
284 same sample W2BD2 (see Table 1) where the most impact on soil porosity was observed.
285 As a result of compaction, the identities of individual aggregates were almost lost and all
286 aggregates seemed to join together to form a single solid mass (see Fig. 2a and b). From
287 these images, it can be directly seen that interpores were strongly reduced (both number
288 and the amount; see Fig. 2c and d) and a sharp increase in number of intrapores (defined
289 here as $< 90 \mu\text{m}$ sized pores) in compacted soils was found (detailed quantified data
290 shown in Sections 3.2–3.4; see Fig. 2e and f).

291

292 *3.2 Effect of soil compaction on total porosity*

293 Using 3D image processing tools, the total pore volume in all samples was
294 calculated with an average of $741 \pm 90 \text{ mm}^3$ ($n = 18$) before compaction and the total
295 pores surface area was on average $6875 \pm 2471 \text{ mm}^2$ ($n = 18$) as shown in Fig. 3. Soil

296 compaction significantly ($P < 0.001$) decreased the total pore volume by ~35% for a net
297 change in bulk density of 0.28 g cm^{-3} (BD1) regardless the soil moisture. Similarly, the
298 effect of added moisture with higher compaction level (W2BD2) also produced significant
299 reduction in the volume of pores by 66% (Fig. 3a). In contrast, the total pore surface area
300 significantly ($P < 0.01$) increased with soil compaction, by ~25% with an increase in bulk
301 density of 0.28 g cm^{-3} (Fig. 3b) and by 37% with an increase in bulk density of 0.71 g cm^{-3}
302 but the difference was not significant ($P = 0.1$). Similar trend was also found for W2BD2
303 treatment; though there was an increase in pore surface area, it was not statistically
304 significant.

305 The resolution of the images used for processing and calculation of pores volume
306 and surface area was $30 \mu\text{m}$. Hence, pores below $30 \mu\text{m}$ were not taken into account in
307 image processing leading to an underestimation of pores, especially of intrapores. In
308 order to estimate the proportion of micropores that was not measured from our analysis
309 due to the resolution, the total porosity obtained from images was subtracted from the
310 total porosity obtained from the bulk density values and particle density of 2.65 g cm^{-3} .
311 These differences ranged from 14.2 to 26.2% (mean value \pm standard deviation was 20.2
312 $\pm 4.3\%$) and represent the missing micropores among the treatments (including before
313 and after compaction). On average this microporosity increased by 6.3% after
314 compaction and was found significant ($P < 0.05$) for W1 BD1 and W2 BD1 but not for W2
315 BD2 (data not shown).

316

317 *3.3. Effect of soil compaction on inter and intrapore size characteristics*

318 In this section, the impact of compaction on interpores and intrapores is presented
319 in two ways; first, by the proportion of inter and intrapores (Fig. 4) and second, by their
320 actual volumes (supplementary material, Fig. S1). Interpores dominated the total pores

321 volume in comparison to the intrapores, representing > 90% of the total pore volume
322 before compaction in pre-compacted samples, however, after compaction there was an
323 increase in intrapores in all cases (Fig. 4a and b). The increase in gravimetric soil water
324 content from 9.3% to 18.3% (w/w) significantly ($P < 0.001$) decreased the proportion of
325 interpores volume by 22% (W1BD1) and 7% (W2BD1) and in the case of W2BD2 the
326 decrease was 59% (Fig. 4a). In all cases, the decrease in interpores produced a
327 corresponding increase in intrapores (Fig. 4b). In the case of surfaces area of inter and
328 intrapores, similar shifts were observed. The proportion of surface area of interpores
329 decreased by approximately 18% in both compaction intensities (i.e. W1BD1 and
330 W2BD1). However, for the treatment with higher water content with higher compaction
331 intensity (W2BD2), the reduction was 39% (Fig. 4c), with a corresponding increase in
332 surface area of intrapores (Fig. 4d). Thus, the effect of compaction on surface area of inter
333 and intrapores was significant ($P < 0.001$). These trends are further illustrated in Fig. S1
334 in their actual values. The interpores volumes decreased by 53% at soil water content
335 9.3% but by 39% with higher soil water content under same compaction intensity
336 (W1BD1 and W2BD1) and by 88% in high moisture and high compaction treatment
337 (W2BD2) (Fig. S1a). In the case of intrapores, their volumes increased significantly ($P <$
338 0.05) by 53% (W1BD1), 58% (W2BD1) and 73% (W2BD2) (Fig. S1b). At higher soil water
339 content, soil compaction did not significantly ($P = 0.77$) affect the interpores surface area,
340 while it was reduced by 20% at low soil water content (Fig. S1c). Strikingly, only high
341 level of soil compaction decreased (by 60%) the interpores surface area while no change
342 was found a low level of compaction (BD1). In contrast, intrapores surface area increased
343 by 44% for W1BD1, 52% for W2BD1 and 66% for W2BD2.

344

345 *3.4. Size distribution of interpores*

346 Fig. 5 shows the changes in the interpores volumes (i.e. volume of individual
347 interpore) before and after compaction along with the changes in the interpores numbers
348 for one replicate. The trends were similar for the different replicates (data not shown).
349 The increase in soil moisture resulted in a higher number of interpores with a volume <
350 0.0001 mm³ (Fig. 5b), in comparison to the low soil moisture samples (Fig. 5a). It is clear
351 from these figures that soil compaction increased the total number of interpores due to
352 the increase in the number of small interpores (< 0.001 mm³), although the total volume
353 of interpores decreased sharply. The number of interpores was on average ($n = 3$), for
354 W1BD1 samples increased from 260 ± 150 before compaction to 695 ± 53 after
355 compaction. For W2 BD1, this change was 59 ± 32 before compaction and 838 ± 60 after
356 compaction whereas for W2 BD2, the number of pores increased from 120 ± 21 before
357 compaction to 670 ± 45 , after compaction. In contrast, the interpores volume was on
358 average ($n = 3$) for W1 BD1 samples 1338 ± 323 mm³ before compaction and 279 ± 18
359 mm³ after compaction, for enhanced soil water content (W2BD1) 2460 ± 1941 mm³
360 before compaction and 494 ± 23 mm³ after compaction, and for high compaction level
361 (W2 BD2) 1465 ± 163 mm³ before compaction and 73 ± 31 mm³ after compaction. The
362 interpores volume was dominated by a single interpore volume (0.0001 mm³) before and
363 after compaction, and representing > 99% of the total volume for W1 BD1 and W2 BD1
364 (Fig. 5, and see Fig. 2c for images). It was only at higher level of soil compaction (W2 BD2),
365 that the proportion of this large interpores was reduced to 70% on average (Fig. 5c).

366

367 *3.5. Simulations of water flow*

368 The LBM simulations were carried out to compare two compaction levels for
369 elevated moisture levels to predict how pore structure influences the water flow. The
370 LBM provides both visualization as well as quantification of the flow through the porous

371 medium. Thus, Fig. 6a shows a cross sectional view of flow rate distribution, simulated
372 by LBM, from the top part of one of the replicates with gravimetric water content 18.3%
373 and bulk density before and after compaction 0.92 and 1.67 g cm⁻³. The images clearly
374 show there was more velocity channels occurring in uncompacted soil samples than after
375 compaction, where the pores were smaller and disconnected from each other.

376 The relationship between the simulated real velocity obtained by LBM and bulk
377 density of all the samples was a negative linear correlation ($R^2 = 0.96$). An increase in bulk
378 density of only 0.3 g cm⁻³ (i.e. from 0.9 to 1.2 g cm⁻³) decreased by 25% the real velocity.
379 However, an increase in bulk density by 0.7 g cm⁻³ (from 0.92 to 1.62 g cm⁻³) nearly
380 stopped the water flow (Fig. 6b).

381

382 **4. Discussion**

383 *4.1 Shifts in interpores - intrapores balance in compacted soils*

384 The data clearly show significant reduction in total pore volume before and after
385 compaction in all treatments with an increase in total pore surface area. However, this
386 data do not provide enough insights into shifts in interpore and intrapore balance in
387 compacted soils. The distinction of interpores and intrapores was found useful to gather
388 better insights into the effect of soil compaction on soil porosity. It was for the first time,
389 such analysis was carried out and the increase of intrapores after compaction was rather
390 surprising. Though intrapores only represent a small fraction of the total pore volume, it
391 is often ignored because it cannot be measured easily. However this work has shown that
392 there is a balance between inter and intrapores in a unit volume of soil and this balance
393 is affected by compaction.

394 The simple method used in segmenting the 3D images to calculate inter and
395 intrapores have been found very useful to understand changes in soil porosity caused by

396 compaction. Intrapores include all pores within aggregates including cavities or “closed”
397 pores. In some cases, large intrapores ($> 90 \mu\text{m}$; Menon, pers. comm., 2011) are found in
398 aggregates; however such cases were not found in our study. The intrapore size threshold
399 ($< 90 \mu\text{m}$) used in this study is very specific and it may vary according to the sample type.
400 Furthermore, the size of the intrapores investigated ranged from 30 to 90 μm , because of
401 the image resolution used in this study. The intrapores $< 30 \mu\text{m}$ were not measured,
402 leading to an underestimation of their volume. It was estimated (see Section 3.2 for
403 details) that 17.1% and 23.4% of intrapores volume was not measured before and after
404 compaction, respectively. Thus, the intrapores represent a significant proportion of the
405 total porosity and hence, future studies should increase the resolution of the images to
406 increase the range of micropores studied and to fully assess their dynamics. It must be
407 also noted that pores are highly irregular in their shapes and sizes and in particular, when
408 aggregates are loosely packed (i.e. before compaction), a few large interpores occupy
409 significant proportion of the pore volume. Hydraulically, this is better for drainage of soil
410 compared to a large number of fragmented pores after compaction.

411 Our data showed that when soil was compacted, intrapores volume and surface
412 areas increased significantly after compaction (Fig. 4) at the expense of interpores; at the
413 same time the number of interpores increased significantly along with its size distribu-
414 tion (Fig. 5). We propose that the following processes would have occurred while
415 compacting the soil aggregates to changes in interpore volume. A minor rearrangement
416 would occur at first followed by rupture of aggregates (the damage was visible at the
417 surface of the samples after compaction applied) when load is applied. The amount of
418 rupture may depend on the strength of aggregates, which is controlled by soil moisture.
419 Dexter (1988) showed that when aggregates are dry (as for W1), they becomes more
420 susceptible to rupture and materials from the ruptures flows into interpore space,

421 reducing the interpore volume significantly, which was found for W1 with a high
422 reduction of interpores (Fig. 4a). If the soil is plastic (e.g. at higher moisture conditions;
423 W2), plastic flow into interpores space will dominate. Thus, the materials from rupture
424 and plastic flow are responsible for the reduction of interpores volume and
425 fragmentation of interpores. In this process, numerous intrapores will be produced, vast
426 majority of them will be very small (e.g. a submicron to few microns in diameter) and
427 therefore to quantify them, ultra-high resolution imaging devices is required. In this
428 study, the resolution of the images was 30 μm , thus, it was not possible to get information
429 about the pores below this size. A shift in pore size distribution towards more interpores
430 and intrapores in compacted soils would force anaerobic conditions in soil, which affect
431 microbial community structure and activity as well as biogeochemical processes (e.g.
432 increase of N_2O emissions) (Keller et al., 2013).

433

434 *4.2 Effect of soil moisture content on soil compaction*

435 The effect of soil compaction coupled with different soil moisture contents was
436 evaluated in this study. Regardless of the effect of compaction, increasing soil moisture
437 increased interpores volume and surface area while decreasing intrapores (Fig. 4). When
438 focusing on the effect of soil moisture on soil compaction intensity, it was interesting to
439 observe that soil compaction at water content of 9.3% (w/w) resulted in a greater
440 reduction of interpores volume compared to 18.3% (w/w) soil water content. This was
441 contrary to the hypothesis that higher soil moisture results in higher deformation of
442 aggregates. However the data support the hypothesis that addition of water caused a
443 considerable increase in soil strength and stability and such behaviour was reported by
444 Greacen (1960). When aggregates were dry (W1), they were more brittle and weak as
445 suggested by Dexter (1988) earlier, thus more compressible compared to elevated

446 moisture level (W2) for the given level of compaction (BD1). This additional shear
447 strength of soil is explained by the force of surface tension between the soil particles
448 when it is slightly moist. However, the application of higher compaction (BD2) could
449 overcome the shear strength and thus lead to more compaction. The uni-axial load tests
450 revealed the load applied to the samples with low moisture content was almost twice the
451 load required to achieve the same level of compaction (BD1) at the higher moisture
452 content (Table 1). A much higher load (530 kPa) was needed to achieve W2BD2 samples.
453 However, it must be noted that multiple impacts during compaction in the experiment
454 could additionally damage the structure of aggregates and reach the studied bulk
455 densities earlier compared to the uni-axial test. The multiple impacts applied would have
456 damaged more the dry samples compared to the moist ones (Dexter, 1988).

457

458 *4.3 Effect of compaction on soil interpore size distribution*

459 When strong compaction was applied to soil aggregates with elevated water
460 content (W2), a substantial reduction of the proportion of interpores volume occurred
461 with a corresponding rise in intrapores volume proportion (Fig. 4a and b); and changes
462 in the surface areas of pores followed a similar trend, but to a smaller extent.
463 Furthermore, it is for the first time, using the X-ray tomography and 3D image analysis,
464 that change in the interpores volume distribution in compacted soils was quantified. The
465 number of pores were increased between 3 to 14 times by compaction, while the volume
466 of pores drastically decreased by 5 to 20 times in compacted soils (Fig. 5). These changes,
467 along with the increase in intrapores, will have implications in gas and water diffusion in
468 soils as demonstrated by LBM simulations. Further- more, such changes are likely to
469 affect soil biology, as mainly small pores (0.001 mm^3) and disconnected from each other
470 are present in compacted soil. Hence, soil compaction could negatively affect fungi

471 because they are mainly located at the surface of aggregates and pores > 10 μm (Chenu
472 et al., 2001), while bacteria will be in pores potentially isolated from nutrient, oxygen and
473 water input reducing their activity.

474

475 *4.4 Effect of compaction on water flow*

476 The LBM was able to predict the magnitude of changes in flow in response to
477 change in bulk density (or porosity) and it enabled simulation of the flow along with the
478 quantification based on the real pore geometry obtained from the X-ray CT scanner. The
479 flow was reduced by 97–99% when bulk density was 1.6 g cm^{-3} . However, it is important
480 to note that LBM considers only saturated flow in segmented pores. The pores below 30
481 μm were ignored, which plays significant role in water flow in unsaturated conditions.
482 Prediction from LBM relies on digitised solid structure and is affected by how precise the
483 real structure is represented. For example, 30 μm images resolution was used in this
484 study, which missed crucial capillaries below this size. Hence, LBM results provide
485 insights into fluid flow and it is used widely for trend analysis and therefore, the
486 predictions need to be verified with real observations when working with soil samples.
487 The model predictions were in good agreement with measurements in a previous study
488 with sand (Menon et al., 2011) probably due to the resolution of the image used (2–3 μm)
489 and poor fluid interactions with sand grains. However, further modelling efforts are
490 necessary to confirm the impact of compaction on unsaturated flow in soils as previously
491 shown by Aravena et al. (2014). Overall, the drastic reduction of water flow does not only
492 increase the risk of soil erosion but also could affect other biogeochemical processes. For
493 example, Li et al. (2002) reported that with an increase in soil BD from 1.00 to 1.60 g cm^{-3} ,
494 total numbers of bacteria, fungi and actinomycetes (measured by plate-counting
495 technique) declined by 26–39% within the same soil mass.

496

497 **5. Conclusions**

498 The aim of the study was to develop a mechanistic understanding of pore system
499 characteristics in compacted aggregates using 3D imaging and modelling tools. The main
500 findings include:

- 501 1. XMT and image processing tools helped to gain deeper understanding of pore system
502 changes in compacted soils. In this study a pore size > 90 μm was sufficient to follow
503 induced changes in soil structure in aggregates.
- 504 2. As a result of compaction, interpore volume and surface area decreased with
505 corresponding increase in intrapores volume and surface area.
- 506 3. Compaction led to significant changes in interpore pore size distribution. The number
507 of interpores increased by 3 to 14 times whereas its volumes were reduced by 5 to 20
508 times in the treatments.
- 509 4. The LBM simulations predicted a steep decline in flow with increase in bulk density. In
510 our studied soil a bulk density larger 1.6 g cm^{-3} would reduce the water flow up to
511 99%.

512 Future compaction studies may include to understand the effect of soil particle
513 size distribution and different moisture contents. It will be useful to measure the load
514 applied prior to the imaging. More importantly, focus must be to understand how changes
515 in pore size distribution in compacted soil affect soil biogeochemical processes.

516

517 **Acknowledgements**

518 We acknowledge funding support from the European Commission FP 7
519 Collaborative Project "Soil Transformations in European Catchments" (SoilTrEC) (Grant
520 Agreement no. 244118) and The White Rose University Consortium Collaboration Fund

521 (2013–14). The authors would like to thank Taru Lehtinen for her help during the
522 fieldwork. The authors would also like to thank Dr. Leslie Coulten for his help and support
523 with the CT scan, and Structure Vision Ltd for providing LBM support. We also thank Ms.
524 Mehrabi for carrying out additional load tests at the University of Leeds. The authors
525 would like to thank two anonymous reviewers for their valuable suggestions to improve
526 the manuscript.

527

528

529 **References**

530 Amézketa, E., 1999. Soil aggregate stability: a review. *J. Sustain. Agric.* 14, 83–151.

531 Aravena, J.E., Berli, M., Ruiz, S., Suárez, F., Ghezzehei, T.A., Tyler, S.W., 2014. Quantifying
532 coupled deformation and water flow in the rhizosphere using X-ray
533 microtomography and numerical simulations. *Plant Soil* 376, 95–110.

534 Banwart, S., 2011. Save our soils. *Nature* 474, 151–152.

535 Blaud, A., Lerch, T.Z., Chevallier, T., Nunan, N., Chenu, C., Brauman, A., 2012. Dynamics of
536 bacterial communities in relation to soil aggregate formation during the
537 decomposition of ¹³C-labelled rice straw. *Appl. Soil Ecol.* 53, 1–9.

538 Bossuyt, H., Six, J., Hendrix, P.F., 2002. Aggregate-protected carbon in no-tillage and
539 conventional tillage agroecosystems using carbon-14 labeled plant residue. *Soil
540 Sci. Soc. Am. J.* 66, 1965–1973.

541 Berli, M., Carminati, A., Ghezzehei, T., & Or, D. 2008. Evolution of unsaturated hydraulic
542 conductivity of aggregated soils due to compressive forces. *Water Resour. Res.* 44.

543 Bronick, C.J and Lal, R. 2005. Soil Structure and management: a review. *Geoderma* 124, 3-
544 22.

545 Carminati, A., Kaestner, A., Hassanein, R., Ippisch, O., Vontobel, P., & Flühler, H. 2007.
546 Infiltration through series of soil aggregates: Neutron radiography and modeling.
547 Adv. Water. Res. 30, 1168–1178.

548 Chenu, C., Hassink, J., Bloem, J., 2001. Short-term changes in the spatial distribution of
549 microorganisms in soil aggregates as affected by glucose addition. Biol. Fertil. Soils
550 34, 349–356.

551 COM (2006) European Commission (online: [http://ec.europa.eu/environment](http://ec.europa.eu/environment/soil/three_en.htm)
552 [/soil/three_en.htm](http://ec.europa.eu/environment/soil/three_en.htm)).

553 Dexter, A.R., 1988. Advances in characterization of soil structure. Soil Tillage Res.,
554 Proceedings 11th Conference of ISTRO: Tillage and Traffic in Crop Production 11,
555 199–238.

556 EEA (2012) Soil Compaction map of EU: [http://www.eea.europa.eu/data-and-](http://www.eea.europa.eu/data-and-maps/figures/soil-compaction-in-europe)
557 [maps/figures/soil-compaction-in-europe](http://www.eea.europa.eu/data-and-maps/figures/soil-compaction-in-europe).

558 FAO (Food and Agricultural Organization)
559 http://www.fao.org/ag/ca/doc/soil_compaction.pdf (accessed on 02.07.2014)

560 Greacen, E.L., 1960. Water Content and Soil Strength. J. Soil Sci. 11, 313–333.

561 Hartemink, A.E., 2008. Soils are back on the global agenda. Soil Use Manag. 24, 327–330.

562 Haynes, R., Swift, R., 1990. Stability of soil aggregates in relation to organic constituents
563 and soil water content. J. Soil Sci. 41, 73-83.

564 Hillel, D., 1998. Environmental Soil Physics: Fundamentals, Applications, and
565 Environmental Considerations, Academic Press Inc. ed. Academic Press, San
566 Diego.

567 Holtz et al (2010) Geotechnical Eng Prentice Hall (2nd Edition) p 174

568 Horn, R., Smucker, A., 2005. Structure formation and its consequences for gas and water
569 transport in unsaturated arable and forest soils. Soil Tillage Res. 82, 5–14.

570 Keller, T., Lamandé, M., Peth, S., Berli, M., Delenne, J.-Y., Baumgarten, W., Rabbel, W.,
571 Radjai, F., Rajchenbach, J., Selvadurai, A.P.S., Or, D., 2013. An interdisciplinary
572 approach towards improved understanding of soil deformation during
573 compaction. *Soil Till. Res.* 128, 61-80.

574 Lair, G.J., Zehetner, F., Hrachowitz, M., Franz, N., Maringer, F.-J., Gerzabek, M.H., 2009.
575 Dating of soil layers in a young floodplain using iron oxide crystallinity. *Quatern.*
576 *Geochronol.* 4, 260-266.

577 Li, C.H., Ma, B.L., Zhang, T.Q. 2002 Soil bulk density effects on soil microbial populations
578 and enzyme activities during the growth of maize (*Zea mays* L.) planted in large
579 pots under field exposure, *Canadian J Soil Sci* 82, 147-154.

580 Menon, M., Yuan, Q., Jia, X., Dougill, A.J., Hoon, S.R., Thomas, A.D., Williams, R.A., 2011.
581 Assessment of physical and hydrological properties of biological soil crusts using
582 X-ray microtomography and modeling. *J. Hydrol.* 397, 47-54.

583 Mooney, S.J., Pridmore, T.P., Helliwell, J., Bennett, M.J., 2012. Developing X-ray Computed
584 Tomography to non-invasively image 3-D root systems architecture in soil. *Plant*
585 *Soil* 352, 1-22.

586 Murphy, C.P., 1986. *Thin Section Preparation of Soils and Sediments.* A B Academic
587 Publishers, Berkhamsted, UK.

588 R Development Core Team, 2013. R: a language and environment for statistical
589 computing.

590 Sexstone, A.J., Revsbech, N.P., Bailey, T.B., Tiedje, J.M., 1985. Direct measurement of
591 oxygen profiles and denitrification rates in soil aggregates. *Soil Sci. Soc. Am. J.* 49,
592 645-651.

593 Shein, E.V. 2005. *Course of Soil Physics (in Russian).* Moscow State Univ. Publ., Moscow.

594 Six, J., Bossuyt, H., Degryze, S., Denef, K., 2004. A history of research on the link between
595 (micro)aggregates, soil biota, and soil organic matter dynamics. *Soil Till. Res.* 79,
596 7–31.

597 Stamati F., N.P. Nikolaidis, S.A. Banwart and W.E. Blum, 2013. A Coupled Carbon,
598 Aggregation, and Structure Turnover (CAST) Model for topsoils, *GeoDerma*, 211,
599 51-64

600 Tisdall, J.M., Oades, J.M., 1982. Organic matter and water-stable aggregates in soils. *Eur. J.*
601 *Soil Sci.* 33, 141–163.

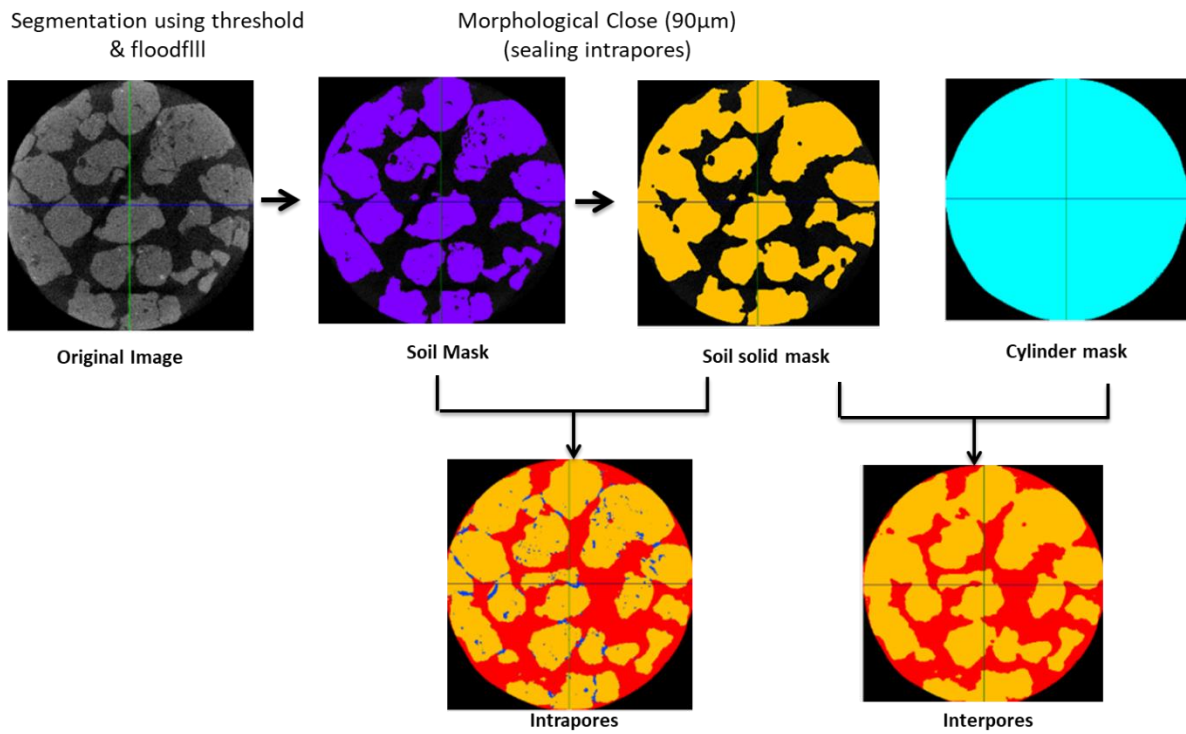
602 **Table 1.** Summary of treatments of the samples including gravimetric water content,
603 initial and final bulk density (before and after soil compaction) and net change in bulk
604 density.

| Treatment Combinations | Gravimetric water content (%) | Initial Bulk Density(g cm ⁻³) | Final Bulk density (g cm ⁻³) | Net change in bulk density (g cm ⁻³) |
|------------------------|-------------------------------|---|--|--|
| W1 BD1 | 9.3 | 0.84 | 1.12 | 0.28 |
| W2 BD1 | 18.3 | 0.92 | 1.20 | 0.28 |
| W2 BD2 | 18.3 | 0.92 | 1.62 | 0.71 |

605

606

607



608

609 **Fig. 1.** A 2D illustration of image processing steps followed in the study to differentiate

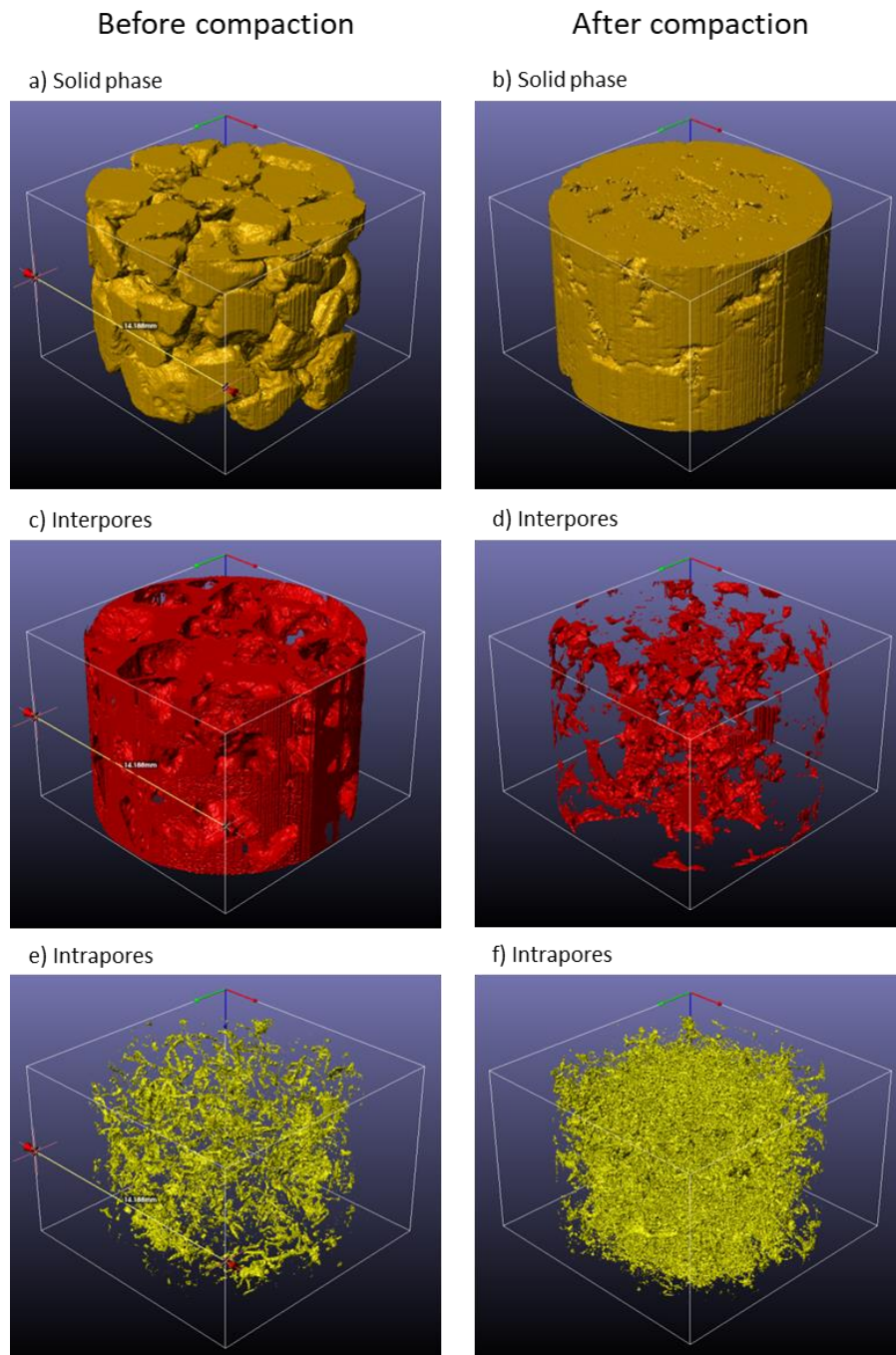
610 interpores and intrapores. The above example is from a replicate before compaction.

611

612

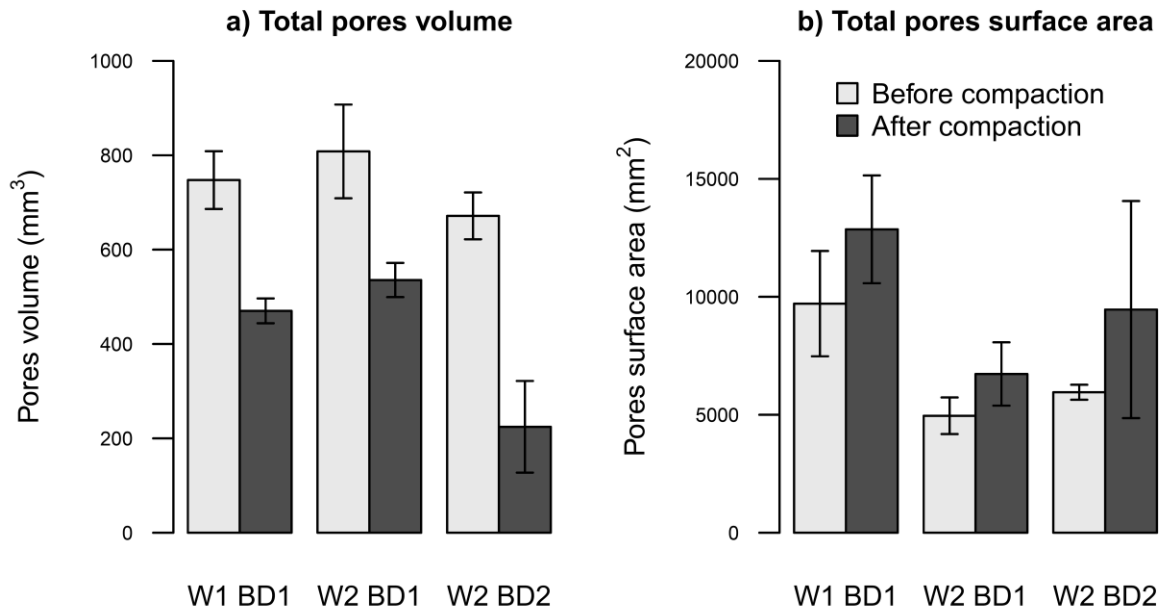
613

614



615

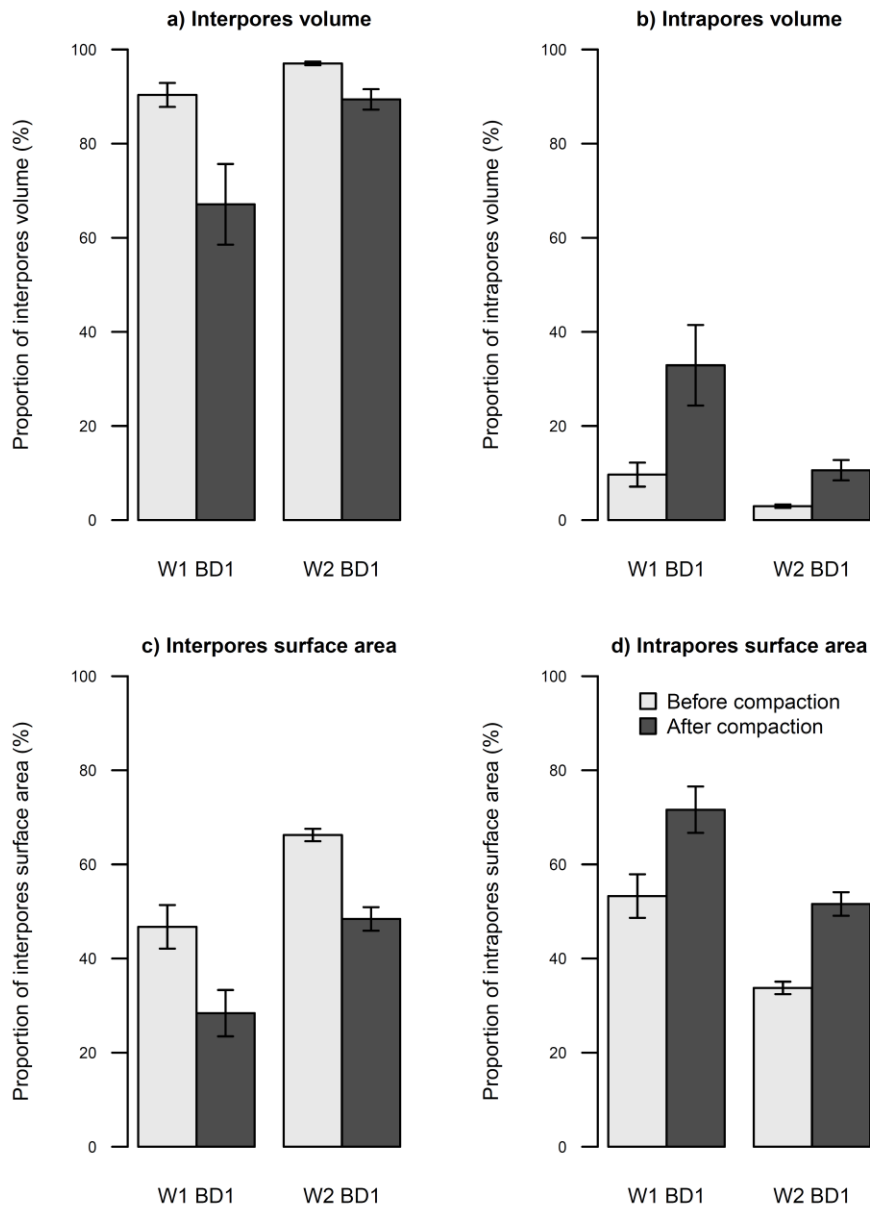
616 **Fig. 2.** 3D view of soil aggregates before and after compaction. The images show the top
 617 1 cm of a replicate from a sample with gravimetric water content 18.3% and bulk density
 618 before and after compaction before and after compaction 0.91 and 1.12 g cm⁻³,
 619 respectively (W2BD2). Images on the left (a, c and e) show the solid phase (gold),
 620 interpores (red) and intrapores (yellow) before compaction, while the images on the
 621 right (b, d, and f) after compaction.



622

623 **Fig. 3.** Effect of soil compaction on total pores volume (a) and surface area (b) on soil
 624 aggregates with varying levels of soil moisture and compaction. Treatments key: W1
 625 refers to moisture content of 9.3% and W2 represents 18.3 % (w/w); BD1 and BD2 refers
 626 to a bulk density increment of 0.28 and 0.71 g cm⁻³, respectively (see Table 1). Means
 627 values ± standard deviation (*n* = 6) are shown.

628



629

630 **Fig. 4.** Effect of soil compaction on interpores (a, c) and intrapores (b, d) volumes (a, b)

631 and surface area (c, d) from soil aggregates with varying levels of soil moisture and

632 compaction. The pores volume and surface area are expressed as proportion (%) of the

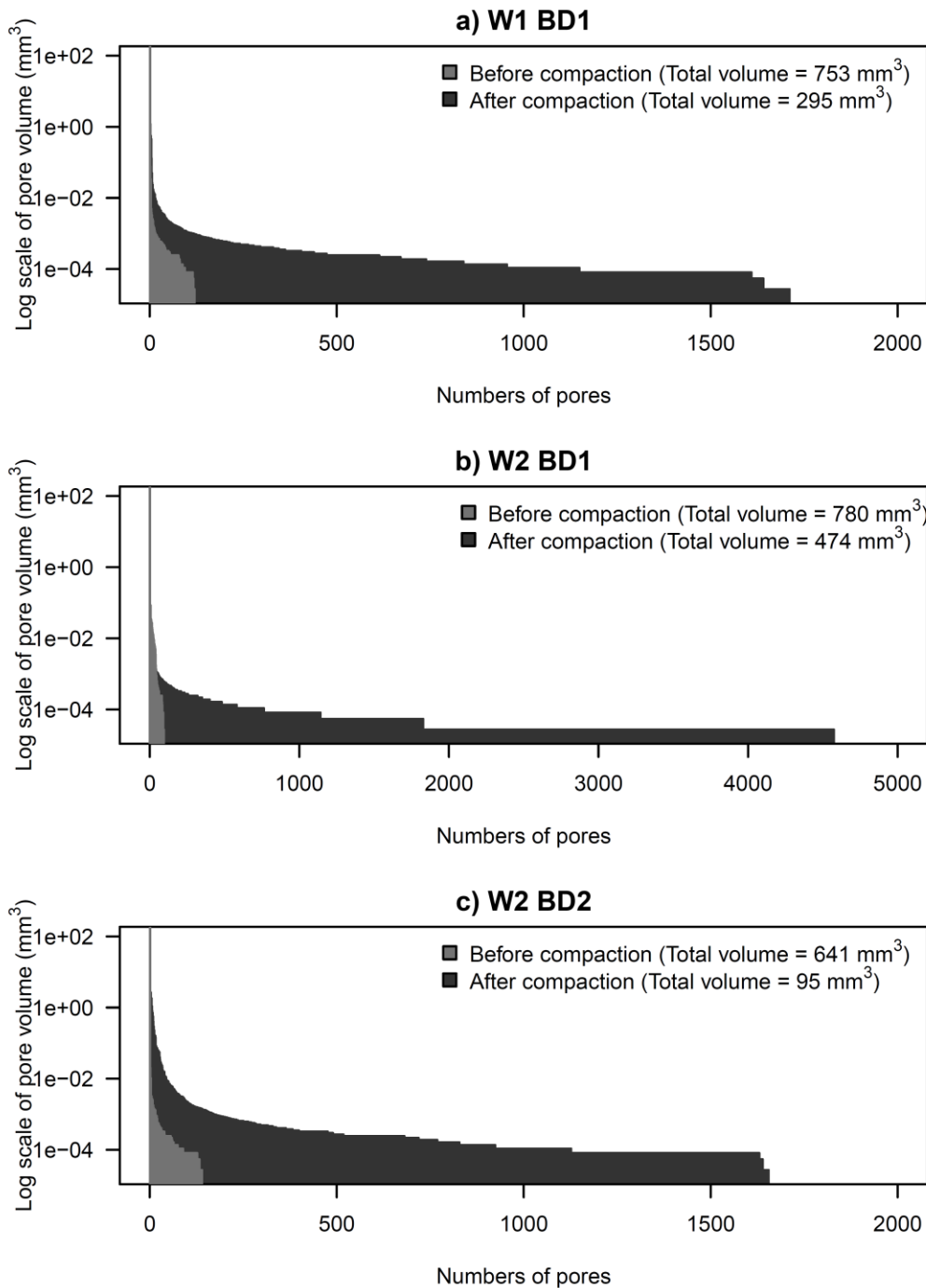
633 total pores (interpores + intrapores) volume and surface area, respectively. Treatments

634 key: W1 refers to moisture content of 9.3% and W2 represents 18.3 % (w/w); BD1 and

635 BD2 refers to a bulk density increment of 0.28 and 0.71 g cm⁻³, respectively (see Table 1).

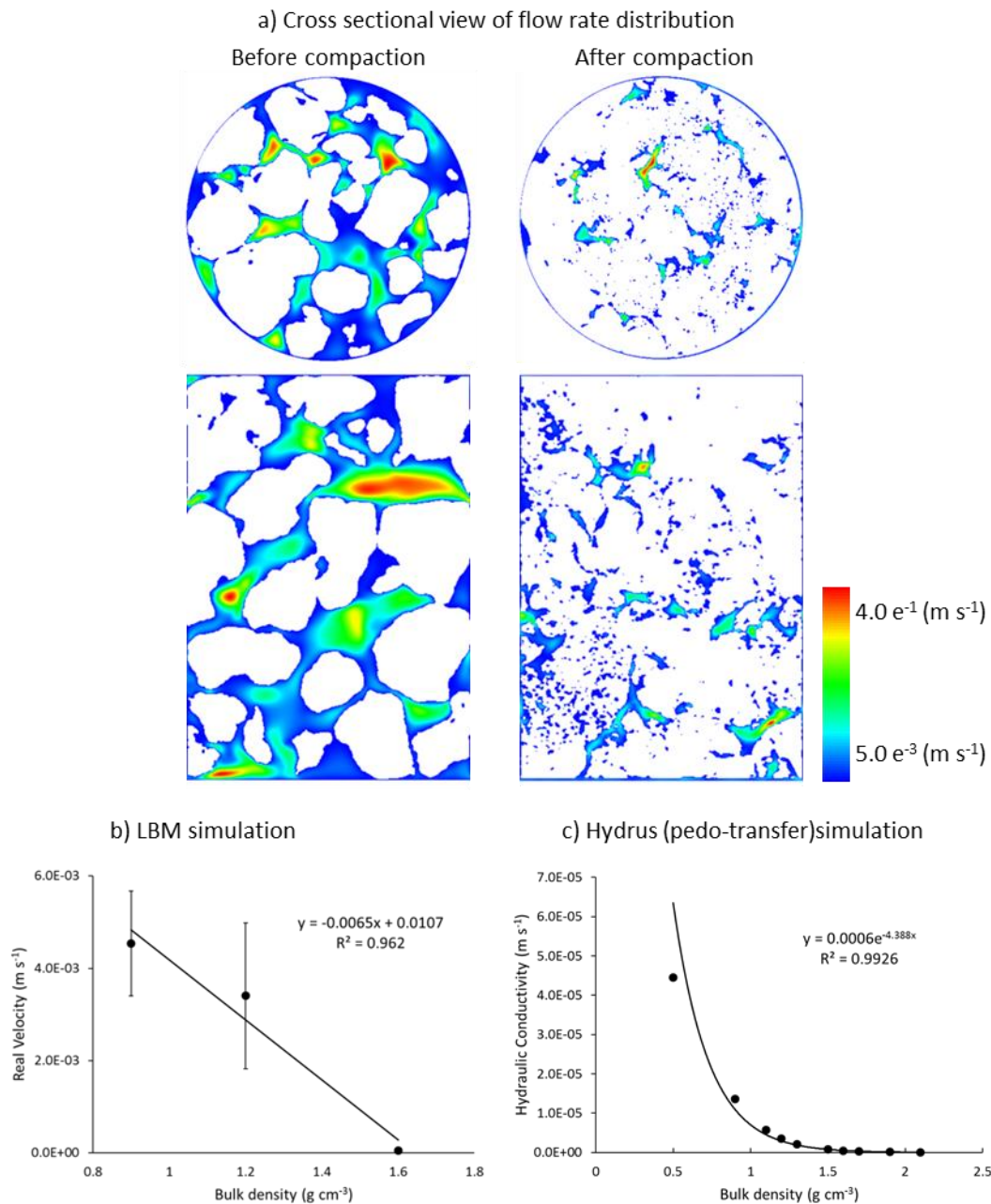
636 Means values ± standard deviation (*n* = 6) are shown.

637



638

639 **Fig. 5.** Distribution of inter-pores volume (mm^3) and their number before (gray) and after
 640 soil compaction (black) in various treatments (a, b and c) applied. Please note that data
 641 from single replicate is shown. Treatment key: W1 refers to moisture content of 9.3% and
 642 W2 represents 18.3 % (w/w); BD1 and BD2 refers to a bulk density increment of 0.28
 643 and 0.71 g cm^{-3} , respectively (see Table 1). NB: For better visualization, we have used a
 644 different scale for X-axis for b.



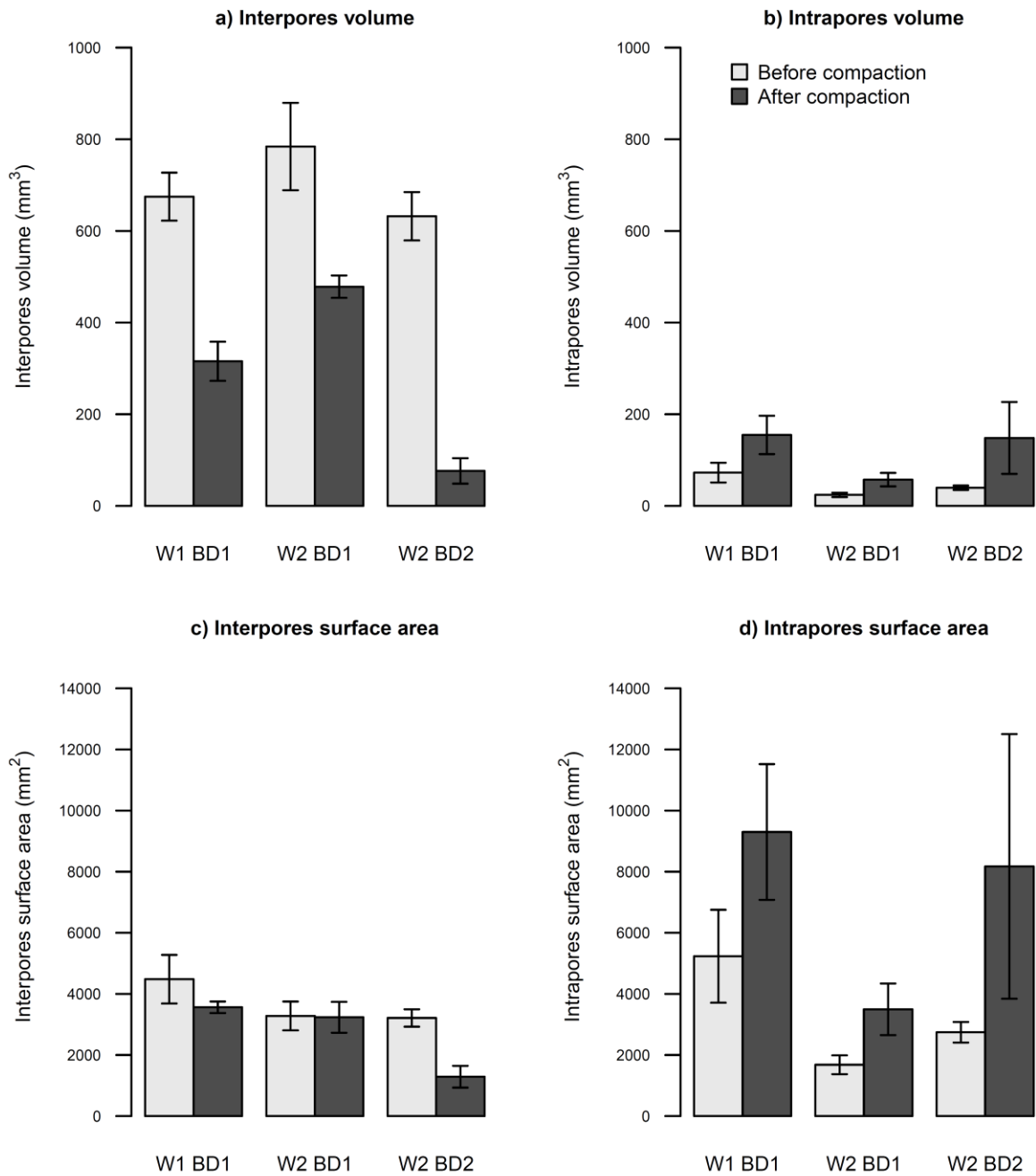
645

646 **Fig. 6.** Results from simulations using LBM; a) 2D cross sectional view of velocity
 647 distributions taken from a replicate with gravimetric water content 18.3% and with an
 648 increment in bulk density of 0.71 g cm^{-3} (W2BD2, see Table 1 for details). Warm colours
 649 indicate higher values of real velocity and the soil appears in white; b) Relationship
 650 between the real velocity obtained by LBM simulations and bulk density (g cm^{-3}) of the
 651 samples with gravimetric water content of 18.3% with changes in bulk density (mean and
 652 standard deviations are shown; $n = 3$, except at bulk density $0.92 \text{ } n = 6$).

653

Supplementary Material

654



655

656 **Fig. S1.** Effect of soil compaction on interpores (a,c) and intrapores (b, d) volumes (a, b) and
657 surface area (c, d) from soil aggregates with varying levels of soil moisture and compaction.

658 Treatments key: W1 refers to moisture content of 9.3% and W2 represents 18.3 % (w/w); BD1

659 and BD2 refers to a bulk density increment of 0.28 and 0.71 g cm⁻³, respectively (see Table 1).

660 Means values ± standard deviation (*n* = 6) are shown.